Macromolecules

Volume 17, Number 6 June 1984

Molecular Motion in Glassy Polystyrenes

Jacob Schaefer,* M. D. Sefcik, E. O. Stejskal, and R. A. McKay

Monsanto Company, Physical Sciences Center, St. Louis, Missouri 63167

W. Thomas Dixon†

Washington University, Department of Chemistry, St. Louis, Missouri 63130

R. E. Cais

AT&T Bell Laboratories, Murray Hill, New Jersey 07974. *Received July 25, 1983*

ABSTRACT: The amplitudes of ring- and main-chain motions of a variety of polystyrenes have been established from the ^{13}C NMR magic-angle spinning sideband patterns of dipolar and chemical shift tensors. The frequencies of the same motions have been determined by $T_1(C)$ and $T_{1\rho}(C)$ experiments. The most prevalent motion in these polymers is restricted phenyl rotation with a sizable average jump angle. Both the amplitude and frequency of this motion vary from one substituted polystyrene to another and from site to site within the same polystyrene. A small fraction of sites within some of the polystyrenes permits high-frequency (megahertz) ring flips in combination with main-chain rotational reorientation, also at high frequency. The concentration of these sites does not depend upon intrachain conformational or configurational defects but rather is determined by interchain glassy-state packing. Low-frequency (kilohertz) main-chain motion is insensitive to ring substitution for some of the polystyrenes, suggesting the presence of a cooperative motion in which the rings only translate as the main chain rotates.

Introduction

The spin–lattice or motional contribution to $T_{1\rho}(C)$ at 37 kHz for polystyrene and various ring- and main-chain-substituted versions of polystyrene has been established[1] by a careful comparison of $\langle T_{1\rho}(C)\rangle$ with the average cross-polarization transfer time from protons in local dipolar fields to carbons in the applied radio-frequency field.[2,3] In each case, molecular dynamics is, in fact, the major contributor to $\langle T_{1\rho}(C)\rangle$. In this paper we report $\langle T_{1\rho}(C)\rangle$'s at 37 kHz for some 12 different polystyrenes. This information, characterizing motion at low frequency, is combined with the results of $T_1(C)$ measurements to define the broad frequency range of polystyrene motion at room temperature.

The amplitudes of these motions can be inferred from the extent of collapse of either chemical shift or dipolar tensors.[5,6] The former is particularly useful for nonprotonated carbons, and, for polystyrenes, can be obtained from a standard magic-angle spinning experiment without recourse to a sideband ordering technique.[7] The collapse of the dipolar tensor is measured by using dipolar rotational sideband echos.[8,9] This 2D-NMR approach has been described before[10] and illustrated by applications to polycarbonate systems.[11] The same methodology will be used here to characterize specific main- and side-chain motions in polystyrenes.

Experiments

Relaxation measurements were made on a spectrometer built around a 12-in. iron magnet operating at a proton frequency of 60 MHz. Half-gram samples were spun with a single-bearing Beams–Andrew[12] type rotor.

The pulse sequence for a combined spin–lattice relaxation experiment is shown in Figure 1. In this experiment, carbon magnetization is generated by cross polarization, held spin-locked in the absence of a decoupling field for a variable time, and then restored to the z-axis direction by a 90° pulse.[13] Following a waiting period comparable to several T_1's of the carbons, the surviving magnetization is sampled by a second 90° pulse. Phase cycling and data routing are employed to ensure normal inversion–recovery behavior.[13] With both $T_{1\rho}(C)$ and $T_1(C)$ delays in the same experiment, it is possible, for example, to measure the megahertz-regime relaxation properties of a fraction of the sites of a dynamically hetereogeneous material, with selection of those sites based on their kilohertz-regime behavior.

The pulse sequence for the dipolar rotational spin-echo experiment is shown in Figure 2. The evolution of the carbon magnetization due to chemical shift effects is refocused after two rotor periods by a carbon 180° pulse applied after the first rotor period. The ^1H–^{13}C dipolar modulation[5,6] is followed by varying the number of phase-shifted multiple-pulse[14] ^1H (WAHUHA) pulse sequences during a time t_1. The spinning speed is chosen

† Present address: Washington University Medical School, Mallinckrodt Institute of Radiology, St. Louis, MO 63110.

0024-9297/84/2217-1107$01.50/0

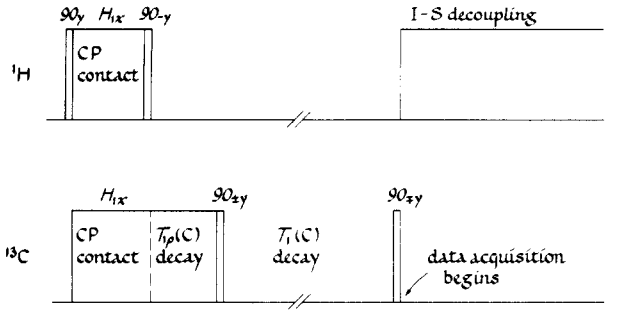

Figure 1. Pulse sequence for a double-select $T_{1\rho}(C)$ and $T_1(C)$ experiment.

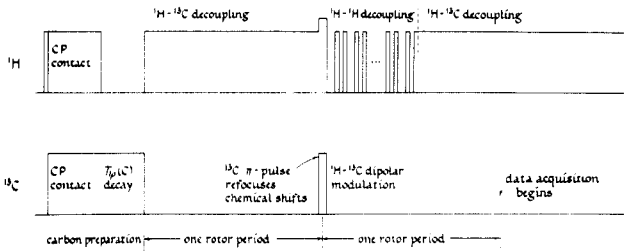

Figure 2. Pulse sequence for a dipolar rotational spin-echo ^{13}C NMR experiment. Following convention, CH dipolar modulation occurs in the time t_1, data acquisition in t_2, and $T_{1\rho}(C)$ decay in t_3.

so that an integral number of WAHUHA cycles exactly fits into one rotor period. In our experiments, this number was 16. Each WAHUHA cycle took 33 μs, with 3-μs 100° pulses,[5] so that sample spinning was at 1894 Hz. Matched spin-lock transfers were performed at 60 kHz. Data acquisition took place during the time t_2. The time t_3 occurred in the preparation part of the sequence during which the carbons were spin-locked in the absence of a decoupling field. This time parameter allows dipolar rotational echos to be obtained from just a part of a sample with selection on the basis of kilohertz-rate relaxation properties. The pulse sequence of Figure 1 is similar to that used by Munowitz et al.[8] and by Munowitz and Griffin[9] for studying dipolar coupling in rotating solids. By inserting the $T_1(C)$ delay of Figure 1 as part of the carbon preparation step shown in Figure 2, it is possible to perform a dipolar rotational echo experiment on a fraction of a sample, with the fraction selected by its megahertz-rate relaxation properties.

Rotational dipolar sideband patterns were simulated by evaluating numerically integrals given by Herzfeld and Berger.[16] Results of these calculations were tested by comparisons to published values.[16] Motionally modified dipolar patterns were calculated by using the Herzfeld and Berger analysis with width and asymmetry parameters evaluated from geometrical considerations under the assumption of fast motion (see the appendix of ref 11).

All substituted polystyrenes were examined as high molecular weight precipitated powders. Atactic and isotactic polystyrene samples were compression molded and examined as both melt-quenched and annealed materials. Atactic polystyrene was supplied by Monsanto Co. Isotactic poly(styrene-α-*d*) was synthesized[17] with 98% enriched monomer (Merck Stable Isotopes, Canada). Stereoregularity of this polymer was greater than 95%. Poly(*p*-bromostyrene), poly(*p*-chlorostyrene), and poly(*p*-nitrostyrene) were supplied by Polysciences, Inc. (Warrington, PA). Poly(*p*-isopropylstyrene) was obtained from Aldrich Chemical Co. (Milwaukee, WI). Poly(α-methylstyrene), poly(*o*-bromostyrene), and poly(*m*-bromostyrene) were provided by Professor Lucien Monnerie and have been described elsewhere.[18] Poly(*p*-*tert*-butylstyrene) and poly(styrene-α-^{13}C), 15 atom % ^{13}C, were synthesized by Dr. R. J. Kern (Monsanto Co., St. Louis, MO). The labeled styrene monomer was provided by Merck Stable Isotopes, Canada.

Results

Line Assignments and Signal Intensities. Magic-angle cross-polarization ^{13}C NMR spectra of main-chain

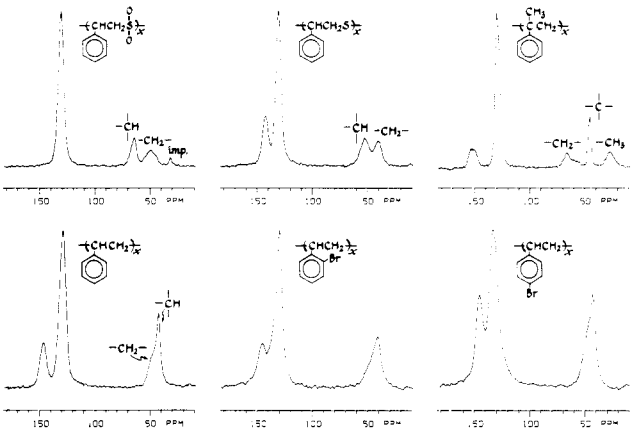

Figure 3. Magic-angle cross-polarization 15.1-MHz ^{13}C NMR spectra of some polystyrenes. Two-millisecond matched spin-lock contacts at 37 kHz were employed.

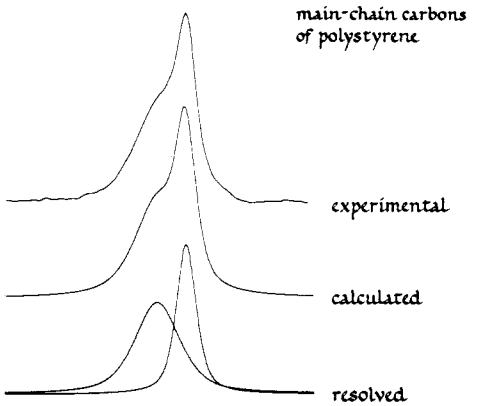

Figure 4. Deconvolution of the aliphatic-carbon resonance of polystyrene into contributions from the methylene and methine carbons.

substituted polystyrenes permit the identification of reasonably well-resolved lines for both the methine and methylene carbons (Figure 3, top row). The unusual line assignments for poly(styrene-*co*-sulfone)[43] and poly(phenylthiirane), $-(CH_2CHPhS)_x-$, are based on solution ^{13}C NMR results.[19,20] The aromatic quaternary-carbon line of poly(styrene-*co*-sulfone) is shifted upfield relative to its usual position and so is not resolved (Figure 3, top left).

The corresponding spectra of ring-substituted polystyrenes are generally less well resolved than that of polystyrene itself (Figure 3, bottom row). Thus, while the resolution of the main-chain aliphatic-carbon resonance of polystyrene can be deconvoluted with a calculated Lorentzian fitting procedure (Figure 4), the main-chain resonance of most ring-substituted polystyrenes must be treated as a combination line.

The observed ratio of integrated aromatic-carbon intensity to aliphatic-carbon intensity for polystyrene is 2.9 compared to an expected value of 3.0. (This discrepancy is due to some aromatic-carbon intensity still contained in the spinning sidebands.) The corresponding ratios for poly(*o*-bromostyrene) and poly(*p*-bromostyrene) are 2.6 and 2.5, respectively. The missing intensity for these two polymers is too large to ascribe to the spinning sidebands. Rather, it seems likely that the brominated aromatic-carbon intensity is missing from the spectra because of severe dipolar broadening of this resonance by a quadrupolar nucleus. Such broadening is not removed by magic-angle spinning.[4]

The ratio of integrated intensity of the protonated to nonprotonated aromatic-carbon resonances of polystyrene is about 4.0, with the ratio of peak heights about 3.5. The

Table I
$\langle T_{1\rho}(C)\rangle$[a] (ms) for the Protonated Carbons of Some Side-Chain Substituted Polystyrenes ($H_1(C)$ = 37 kHz with Magic-Angle Spinning at 2 kHz)

polymer	aliphatic carbons	aromatic carbons
poly(*p*-*tert*-butylstyrene)	5.9	6.2
poly(*p*-isopropylstyrene)	7.5	8.8
poly(*p*-bromostyrene)	5.8	11.0
polystyrene[b]	8.0	11.2
poly(*p*-chlorostyrene)	8.8	14.0
poly(*p*-nitrostyrene)	12.0	19.2
poly(*o*-bromostyrene)	5.2	30.8
poly(*m*-bromostyrene)	7.4	31.1
poly(*o*-chlorostyrene)	7.2	37.0

[a] From straight-line fit to decay between 0.05 and 1.0 ms after the turn off of $H_1(H)$. [b] Atactic, melt-quenched, high-molecular-weight material.

difference between 4.0 and the theoretical value of 5.0 is primarily due to spin dynamics during the matched Hartman–Hahn transfer. As shown in ref 2 (eq 8), after a long contact time, t, the observed carbon magnetization is given approximately by $(T_{1\rho}(H)/(T_{1\rho}(H) - T_{IS})S_M \exp(-t/T_{1\rho}(H))$, where S_M is the magnetization that would be observed in the absence of any dissipative processes. For protonated carbons the preexponential factor involving the relaxation times is nearly unity and can be ignored. For nonprotonated carbons with a distributed T_{IS} (having an average of about 0.5 ms), this factor leads to an overemphasis of intensity. Deducing accurately absolute intensities in this situation requires a curve-fitting process.[2] The overemphasis of nonprotonated carbon intensity is most severe for those polystyrenes with short $T_{1\rho}(H)$'s. Polystyrene itself has a value of under 5 ms and falls in this category. The protonated aromatic-carbon intensity lost during the latter part of the cross-polarization tranfer is due to a single-rate process and so no site in a dynamically heterogeneous polymer is discriminated against.

$T_{1\rho}(C)$ and $T_1(C)$. Values for $\langle T_{1\rho}(C)\rangle$ for ring-substituted polystyrenes are reported in Table I. The protonated aromatic-carbon $T_{1\rho}$ changes by about a factor of 6 with substitution, while the average main-chain (methine plus methylene carbon) values are insensitive to substitution. Both types of $\langle T_{1\rho}(C)\rangle$'s change with alterations of the main chain, however (Table II). Methyl-carbon $T_{1\rho}$'s for the ring-methyl substituted polystyrenes are of the order of 100 ms at 37 kHz, much longer than the aromatic and main-chain values. While the methyl-carbon $T_{1\rho}$ of poly(α-methylstyrene) is comparable in value to aromatic and main-chain $T_{1\rho}(C)$'s at 37 kHz (Figure 5, top), it has a much weaker $H_1(C)$ dependence (Table V, ref 1). Thus for all these polystyrenes at room temperature, methyl groups can be ruled out as having a significant influence on aromatic and main-chain $\langle T_{1\rho}(C)\rangle$'s. Typical $T_{1\rho}(C)$ plots illustrate the quality of the data and the

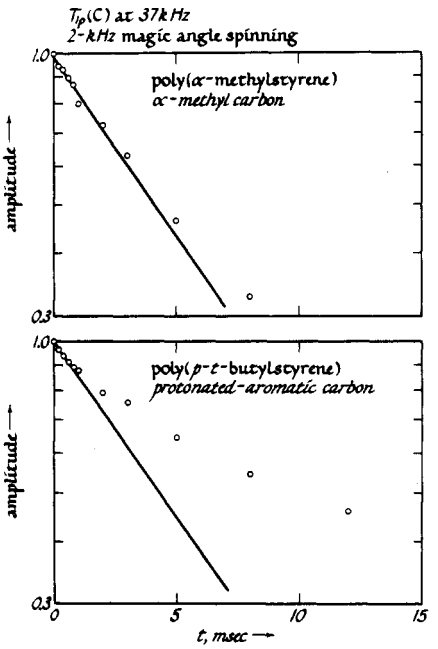

Figure 5. $T_{1\rho}(C)$ plots for individual carbons of two polystyrenes. Variations in packing can give rise to different regions in the glass, each with its own characteristic dynamic properties. This results in a pronounced dispersion or nonlinearity in the $T_{1\rho}(C)$ plot. When local motion is responsible for $T_{1\rho}(C)$, as is the case for the methyl carbon of poly(α-methylstyrene), the dispersion is more modest. For crystalline materials where $T_{1\rho}(C)$ relaxation is due to spin dynamics, the dispersion is almost nil. (See Figure 6 of ref 1.)

Table II
$\langle T_{1\rho}(C)\rangle$[a] (ms) for the Protonated Carbons in Some Main-Chain Substituted Polystyrenes ($H_1(C)$ = 37 kHz with Magic-Angle Spinning at 2 kHz)

polymer	methylene carbon	methine carbon	aromatic carbon
polystyrene	5.2[b]	10.1[b]	11.2
poly(phenylthiirane), $-(CH_2CHPhS)_x-$	5.2	11.3	10.3
poly(styrene-*co*-sulfone), $-(CH_2CHPhSO_2)_x-$	12.0	24.0	22.0[c]
poly(α-methylstyrene)	2.5		19.0

[a] From straight-line fit to decay between 0.05 and 1.0 ms after the turn off of $H_1(H)$. [b] From computer deconvolution of δ_C = 45 resonance (Figure 4). [c] Includes contribution from nonprotonated aromatic carbon.

Table III
Field Dependence of $\langle T_{1\rho}(C)\rangle$ for the Protonated Aromatic Carbons of Some Polystyrenes

	$\langle T_{1\rho}(C)\rangle$,[a] ms			
polymer	$H_1(C)$ = 37 kHz	$H_1(C)$ = 44 kHz	$H_1(C)$ = 54 kHz	$H_1(C)$ = 60 kHz
isotactic polystyrene[b]	13.6	18.1	27.1	31.0
atactic polystyrene[c]	11.2	18.9	19.7	21.7
poly(*p*-methylstyrene)	11.7	18.1	19.6	20.7
poly(*p*-isopropylstyrene)	8.8	12.8	14.5	14.5
poly(*p*-*tert*-butylstyrene)	6.2	8.9	10.0	10.0

[a] Straight-line fit to observed decay between 0.05 and 1.00 ms after the turnoff of $H_1(H)$. [b] Precipitated from decalin. [c] Melt-quenched, high-molecular-weight material.

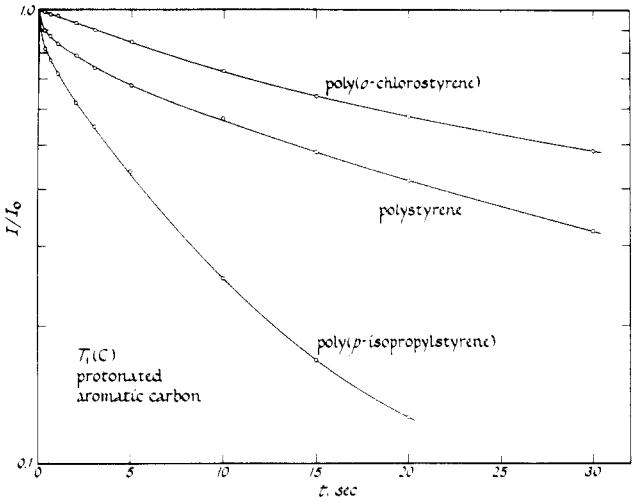

Figure 6. 15.1-MHz T_1(C) plots for three polystyrenes obtained with the pulse sequence of Figure 1 with no $T_{1\rho}$(C) delay. Since the carbon polarization is generated by cross polarization, the repolarization time of the experiment is determined by the short T_1 of the protons.

Table IV
T_1(C) (s) Spin-Lattice Relaxation Times for Some Polystyrenes at 15.1 MHz

polymer	protonated aromatic carbon	methyl carbon[a]
poly(*p*-isopropylstyrene)	0.06 (short) 10 (long)	0.54
poly(*p*-*tert*-butylstyrene)	0.05 (short) 12 (long)	0.46
polystyrene[b]	0.06 (short) 25 (long)	
poly(α-methylstyrene)	7[c]	0.019
poly(*o*-chlorostyrene)	30[c]	

[a] Average value; straight-line fit over first 10% decay. [b] Atactic, melt-quenched, high-molecular-weight material. [c] Average value.

method[2,3] of estimating the average $T_{1\rho}$(C) by the initial slope (Figure 5).

The field dependences of $\langle T_{1\rho}(C)\rangle$ for the protonated aromatic carbons of some polystyrenes are presented in Table III. The dependence for the four glassy polymers is the same. For all of these $\langle T_{1\rho}(C)\rangle$'s (which include the shorter values of Table I), the H_1(C) dependence above about 50 kHz is nil. This is in contrast to the $\langle T_{1\rho}(C)\rangle$'s of entries near the bottom of Table I, which have a field dependence over the full range examined (Table V, ref 1).

Just as with the $T_{1\rho}$(C) plots, the T_1(C) plots for the protonated aromatic carbons of polystyrene and poly(*p*-isopropylstyrene) are highly curved (Figure 6). The short T_1(C) component of these plots is of the order of 50 ms, as short as T_1(C)'s for polymers in solution. However, the long-T_1(C) component is at least 20–30 s, resulting in a dispersion of 3 orders of magnitude (Table IV). After 30 s some 40% of a typical polystyrene solid is still unrelaxed. Short- and long-T_1(C) components do not exchange. For poly(*p*-*tert*-butylstyrene) and poly(*p*-isopropylstyrene), the T_1(C) plots clearly have more than two components, while for poly(*o*-chlorostyrene), poly(α-methylstyrene), and poly(styrene-*co*-sulfone), only a single component may be present (Figure 6). A two-component T_1(C) with a broad dispersion is also observed for the main-chain methine carbon of polystyrene (Figure 7).

Removing the short-T_1(C) population from polystyrene and poly(*p*-*tert*-butylstyrene) by the method of Figure 1

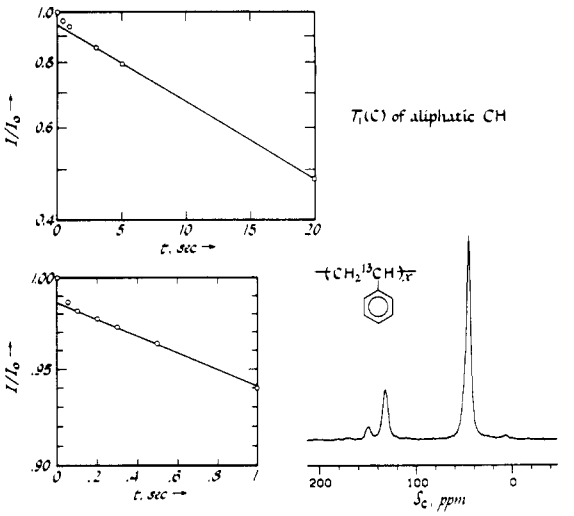

Figure 7. 15.1-MHz methine-carbon T_1(C) plots for poly(styrene-α-^{13}C) obtained with the pulse sequence of Figure 1 with no $T_{1\rho}$(C) delay. The 15 atom % enrichment of the methine carbon improves the sensitivity of the T_1(C) experiment and also makes possible the determination of a dipolar sideband pattern with no interferences from methylene carbons (cf Figure 10).

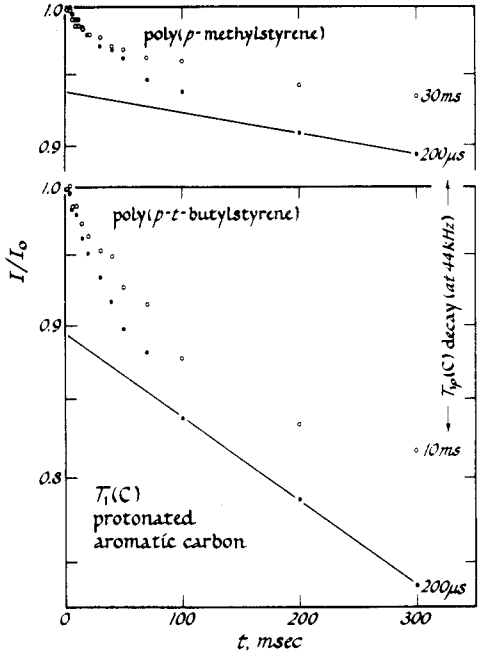

Figure 8. 15.1-MHz T_1(C) plots for two polystyrenes obtained with the pulse sequence of Figure 1 with 200-μs and 30-ms $T_{1\rho}$(C) delays with H_1(C) = 44 kHz. For both polymers, removal of the short-$T_{1\rho}$(C) component produces a minor decrease in the rate of T_1(C) relaxation.

Table V
$\langle T_{1\rho}(C)\rangle$[a] (ms) (at 44 kHz) for Protonated Aromatic Carbons of Two Polystyrenes

polymer	T_1(C) delay,[b] ms			
	2	20	80	300
atactic polystyrene,[c] melt quenched	18.5	18.6	18.3	24.8
poly(*p*-*tert*-butylstyrene)	8.6	8.9	9.4	11.5

[a] Straight-line fit to observed decay between 0.05 and 1.0 ms after the turn off of H_1(H). [b] As defined in Figure 1. [c] High-molecular-weight material.

has a measurable but minor effect on the $T_{1\rho}$(C)'s of those polymers (Table V). This means the motion responsible for the 50-ms T_1(C)'s is not the major contributor to the protonated aromatic $T_{1\rho}$(C)'s, not a surprising result.

Table VI
Mole Fraction of Ring Carbons Contributing to Short-T_1(C) Component for Various Polystyrenes

treatment or substitution	$f(c)$[a]
atactic polystyrene (MW ~ 200 000)	
melt quenched	0.07
annealed ($T < T_g$) and air cooled	0.07
annealed ($T > T_g$) and oven cooled	0.07
precipitated from tetrahydrofuran	0.08
cast from cyclohexane (T = 35 °C)	0.07
atactic polystyrene (MW ~ 1400)	0.10
isotactic polystyrene (MW ~ 100 000)	
melt quenched	0.08
annealed ($T > T_g$)	0.06
precipitated from decalin ($T < T_g$)	0.04
poly(*p*-bromostyrene)	0.06
poly(*p*-methylstyrene)	0.07
poly(*p*-isopropylstyrene)	0.10
poly(*p*-*tert*-butylstyrene)	0.11
poly(*o*-chlorostyrene)	0.00
poly(α-methylstyrene)	0.00
poly(styrene-*co*-sulfone)	0.00

[a] Estimated from curvature of T_1(C) plots (see Figure 6 and associated text).

Similarly, the short-T_1(C) behavior of these polymers is not eliminated by removing the fraction of the sample most efficiently relaxed on a $T_{1\rho}$(C) scale (Figure 8).

Because the observed $\langle T_{1\rho}(C)\rangle$ increases on removal of the short-T_1(C) component, the short-T_1(C) component itself has a short $\langle T_{1\rho}(C)\rangle$. Comparing $\langle T_{1\rho}(C)\rangle$'s after T_1(C) delays of 2 and 300 ms, respectively, in Table V, we see that removing the 10% of the ring population with the shortest T_1(C) increases by 20% the $\langle T_{1\rho}(C)\rangle$ of the remaining rings. The $\langle T_{1\rho}(C)\rangle$ of the short-T_1(C) component is therefore on the order of 7 ms.

The fraction of carbons in various polystyrenes contributing to the short-T_1(C) component can be estimated from extrapolations to zero time of slopes determined at longer times. Since the polystyrene plots are multicomponent, we chose to base these extrapolations on relaxation behavior at comparable parts of each curve, near 1 s for the aliphatic carbons (Figure 7, top left) and 300 ms for the aromatic carbons (Figure 8). This procedure will yield an estimate for the concentration of only the fastest T_1(C) component. These concentrations for the phenyl rings of various polystyrenes are presented in Table VI and identified as $f(c)$. These values vary from a low of 0% for poly(*o*-chlorostyrene) to a high of 11% for poly(*p*-*tert*-butylstyrene). For glassy polystyrene itself, $f(c)$ is independent of tacticity and thermal history, and only weakly dependent on molecular weight. Isotactic polystyrenes with some crystallinity, however, have a reduced value of $f(c)$.

Dipolar Modulation. Some chemical-shift spectra as a function of WAHUHA irradiation for poly(styrene-*co*-sulfone) are shown in Figure 9 (left). Protonated carbon magnetization rapidly dephases under as little as two cycles of WAHUHA irradiation but is refocused after sixteen cycles (one rotor period). Magic-angle spinning should refocus dipolar coupling just as it does chemical shift anisotropy, so in principle, an echo refocused following one rotor period of dipolar modulation should have the same intensity as one without any dipolar modulation.[10] In fact, the former echo is only a third to a half as large. The losses are due primarily to incomplete ^{1}H–^{1}H decoupling.

Using 16 separate chemical-shift spectra (the number of WAHUHA cycles varying from zero through fifteen),[10] we performed 16-point Fourier transforms with the WAHUHA irradiation period as the time variable and peak heights as the intensity variable. The resulting transforms

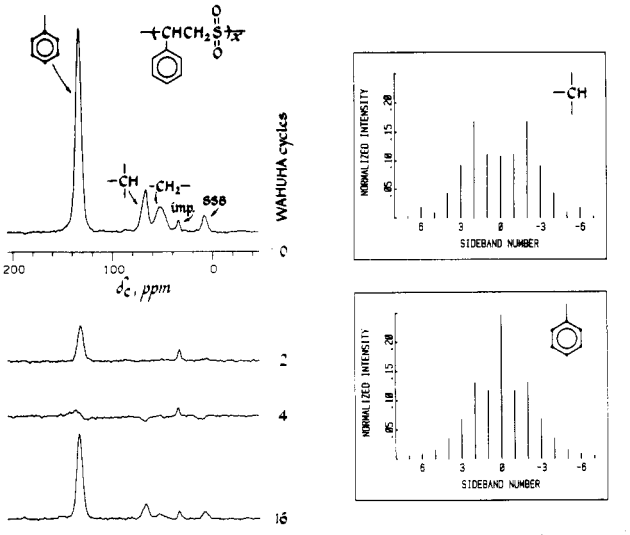

Figure 9. Dipolar rotational spin-echo 15.1-MHz ^{13}C NMR spectra of poly(styrene-*co*-sulfone) at room temperature as a function of the number of WAHUHA cycles used during ^{1}H–^{13}C dipolar evolution (left). Experimental dipolar sideband patterns for the two CH pairs of the polymer under magic-angle spinning at 1.894 kHz are shown at the right of the figure. The intense centerband in the aromatic-carbon dipolar pattern arises from contributions from the nonprotonated carbon whose isotropic chemical shift is accidentally the same as that of the protonated aromatic carbons.

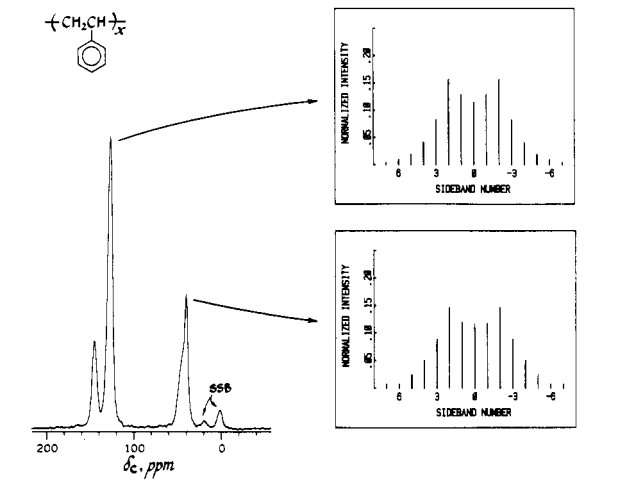

Figure 10. Experimental dipolar sideband patterns for aromatic CH (top) and aliphatic CH (bottom) pairs under magic-angle spinning at 1.894 kHz for melt-quenched atactic polystyrene.

for two carbons of poly(styrene-*co*-sulfone) are shown in Figure 9 (right). To a good approximation, the dipolar pattern of the aliphatic CH pair is a Pake doublet broken into spinning sidebands separated by 1.894 kHz. Each sideband is represented by a single point in the frequency domain. Intensities of the sidebands can be reliably compared so long as sideband shapes are the same. The dipolar sideband pattern for the aromatic-carbon line is similar to that of the aliphatic methine carbon, except for the appearance of a pronounced centerband. This is not an artifact. The centerband intensity arises from a contribution by the nonprotonated aromatic carbon. With no directly bonded proton, carbon–proton dipolar interactions are weak, and the sideband pattern for this carbon is contained predominantly (but not exclusively) in the centerband.

Dipolar sideband patterns for aromatic and aliphatic CH pairs of polystyrene are similar (Figure 10). Both have more intensity in the zeroth and first sidebands, and less in the second sideband, than does the corresponding

Table VII
Comparisons of Calculated and Experimental Dipolar Rotational Sideband Intensities for Some Polystyrenes with Magic-Angle Spinning at 1894 Hz

polymer	CH pair		experiment or motional model	sideband number 0	1	2	3	4	5
poly(*p*-isopropylstyrene)	aromatic	1	obsd[a]	0.138	0.142	0.153	0.079	0.038	0.014
		2	obsd, short-T_1(C) component removed	0.129	0.135	0.156	0.083	0.041	0.015
		3	calcd, C_2 rolls, θ(rms) = 21°	0.134	0.153	0.178	0.063	0.028	0.009
		4	calcd, motion on a sphere, θ(rms) = 19°	0.134	0.157	0.178	0.060	0.027	0.008
poly(styrene-*co*-sulfone)	aliphatic	5	obsd[b]	0.104	0.110	0.164	0.091	0.045	0.012
		6	calcd, static	0.120	0.124	0.185	0.075	0.038	0.013
atactic polystyrene,[c] short-T_1(C) component	aromatic	7	obsd[d]	0.222	0.208	0.127	0.047	0.007	0.000
		8	calcd, C_2 180° flips[e]	0.198	0.213	0.128	0.033	0.014	0.004
		9	calcd, Tonelli conformational distribution[f]	0.259	0.215	0.108	0.033	0.011	0.003

[a] From Figure 3, ref 10. [b] From Figure 9, top right. [c] Melt-quenched, high-molecular-weight material. [d] From Figure 11, top left. [e] From Figure 11, top right, but with 20% contribution from static para CH pair. [f] Reference 21.

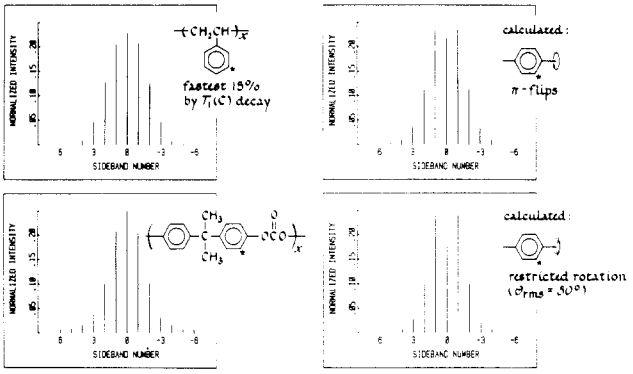

Figure 11. Experimental dipolar sideband patterns for the protonated aromatic carbon of the short-T_1(C) component of polystyrene (upper left) under magic-angle spinning at 1.894 kHz. The pattern is qualitatively similar to that observed for polycarbonate (lower left). The latter has been shown to be partially collapsed by large-amplitude molecular motion. Calculated dipolar patterns for the aromatic starred carbons, based on two different assumptions about motion, are shown at the right of the figure.

pattern for the aliphatic CH pair of poly(styrene-*co*-sulfone). The aliphatic CH pattern for polystyrene was obtained by using a chemical shift position corresponding to the half-height of the right-hand side of the high-field line (near 40 ppm). Virtually the identical pattern was observed for the aliphatic CH pair of poly(styrene-α-^{13}C). In the latter case, there is no possibility of a significant contribution from methylene carbons to the methine CH dipolar sideband pattern.

The dipolar sideband pattern for the short-T_1(C) component of polystyrene (Figure 11, top left) is significantly different from that for the entire sample. Over 60% of the total sideband intensity is contained in the zeroth and first sidebands. This pattern is similar to that observed for polycarbonate (Figure 11, bottom left), a polymer whose rings have been established to undergo large-amplitude molecular motion.[11]

Calculated Dipolar Sideband Patterns. The polystyrene dipolar patterns shown in Figures 10 and 11 are not Pake doublets reflecting only the CH static dipolar coupling (as scaled by WAHUHA irradiation of the protons). Rather, the patterns have been narrowed by molecular motion. Using the methods developed by Herzfeld and Berger[16] and described in detail in the appendix of ref 11, we calculated how ring motion of various types (restricted ring rotations at a rate fast compared to the dipolar coupling) affect the dipolar sideband patterns. Restricted rotation of an aromatic CH vector about the ring C_2 axis

Table VIII
Calculated Ratio of Second to First Dipolar Rotational Sideband Intensities for a CH Pair Undergoing Molecular Motion and Magic-Angle Spinning (1894 Hz)

motional model	total azimuthal angular displacement, deg	n_2/n_1
restricted ring rotation[a]	0	1.50
	20	1.44
	40	1.35
	60	1.16
	80	0.93
	100	0.70
	120	0.53
	140	0.41
ring π flips	180	0.48

[a] Aromatic CH vector undergoing fast diffusional reorientation on the surface of a 60° cone.

(motion lying on a 60° cone) produces a reduction in intensity of the second, and increases in the zeroth and first dipolar sidebands, with respect to the static pattern (Table VII, rows 3 and 6). For poly(*p*-isopropylstyrene), motion of this type with a root-mean-square rotation angle of about 20° produces a reasonable fit with experiment (Table VII, rows 2 and 3). The choice of motional model is not crucial for these sorts of small-angle excursions. Motion of the CH vector on a sphere rather than a 60° cone gives a similar result (Table VII, row 4).

As mentioned earlier, a calculated static Pake pattern gives a resonable fit to the observed methine CH pattern for poly(styrene-*co*-sulfone) (Table VII, rows 5 and 6). This is in contrast to the drastically altered aromatic-carbon pattern for the short-T_1(C) component of atactic polystyrene. The latter is fit by large-amplitude C_2-axis rolls (Figure 11, bottom right) or by 180° flips mixed in with smaller oscillations (Table VII, row 9). The latter motion corresponds to wiggling near the bottoms of a double-minimum potential well with frequent jumps over the top, but with little time spent near the top of the barrier.[21] The pattern calculated for 180° flips alone does not quite match; in particular, the centerband intensity is weaker than observed (Figure 11, top right).

Since the second dipolar spinning sideband is near the cusps of the CH Pake doublet (reduced by WAHUHA decoupling), the ratio of intensities of the second to first sidebands is a sensitive monitor of partial collapse of the dipolar tensor by restricted molecular motion. With a

Table IX
Relaxation Parameters for Protonated Aromatic Carbons with Magic-Angle Spinning at 1894 Hz

system	37-kHz $\langle T_{1\rho}(C)\rangle$,[a] ms	$f(c)$[b]	n_2/n_1[c]	$[n_2/n_1]_d$[d]	$[n_2/n_1]_d$*[e]
melt-quenched atactic polystyrene[f]	11	0.07	1.20	1.31	1.37
isotactic polystyrene					
melt quenched	12	0.08	1.17	1.22	1.28
annealed ($T > T_g$)	28	0.06	1.27	1.33	1.38
precipitated from decalin	14	0.04	1.36	1.37	1.41
crystalline *p*-isopropoxybenzoic acid	83	0.00	1.39	1.39	1.39

[a] Straight-line fit to observed decay between 0.05 and 1.00 ms after the turn off of H_1(H). [b] Mole fraction of rings undergoing megahertz-rate flips as determined by T_1(C) and dipolar modulation results. [c] Ratio of intensities of second to first dipolar rotational sidebands. [d] Ratio of intensities of second to first dipolar rotational sidebands after a 30-ms ^{13}C spin-lock delay at 60 kHz; the subscript refers to this delay. [e] Ratio of intensities of second to first dipolar rotational sidebands after a 30-ms ^{13}C spin-lock delay at 60 kHz with contributions from rings undergoing megahertz-rate 180° flips removed. [f] High-molecular-weight material.

choice of scaling factor[10] to give a static ratio of n_2/n_1 sidebands of 1.50, the effect of C_2-axis rotation of increasing amplitude is shown in Table VIII. A total angular excursion of 120° ($\theta_{rms} = 60°/2^{1/2} = 42°$) reduces n_2/n_1 by a factor of 3, about the reduction achieved by 180° flips.

Chemical Shift Tensor. In general, it is not possible to distinguish the presence of large-amplitude C_2-axis rolls from that of 180° C_2-axis flips using the extent of collapse of the dipolar (or quadrupolar) tensor of off-axis carbons (or their attached deuterons).[11] This is especially true in dynamically heterogeneous materials where dipolar and quadrupolar line shapes can be complicated by the presence of contributions from C_2-axis free rotors.

The distinction between the two motional models can be made by using the extent of collapse of the chemical shift tensor of the on-axis carbons. We assume the principal components of this tensor lie exactly along the bond symmetry axes. The chemical shift tensor is unaffected by 180° flips but is averaged considerably by large-amplitude rolls.[22] For melt-quenched isotactic poly(styrene-α-*d*), the nonprotonated on-axis carbon resonance is well resolved (145 ppm, Figure 12). The spectrum of Figure 12 was taken at low spinning speed to generate large spinning sidebands and so simplify the evaluation of chemical shift anisotropy parameters. The first spinning sidebands of the nonprotonated aromatic-carbon resonance appear at 75 and 215 ppm. Each of these sidebands is flanked on the right by a larger spinning sideband of the protonated aromatic-carbon line. The resonance of the methylene carbon appears at about 45 ppm. The broad peaks at 105 and 175 ppm are spinning sidebands from the deuterated methine carbon.

The deuterated version of this polymer was used so that selection by T_1(C) relaxation for the nonprotonated ring carbon would be dominated by the motion of ring protons. The only main-chain proton in normal isotactic polystyrene that has proximity to the nonprotonated ring carbon is the methine proton.[23] At the same time, the dynamics of the rings of quenched isotactic polystyrene and atactic polystyrene (as reflected in carbon relaxation parameters) are similar (Table IX, rows 1 and 2). The short-T_1(C) selected version of the spectrum is shown in Figure 12 (top). The upper and lower first spinning sidebands are just as intense relative to the isotropic peak for the nonprotonated carbon in this spectrum as in that of the full sample. There is no significant averaging by molecular motion of the chemical shift tensor, and, therefore, large-amplitude C_2-axis rolls can be rulted out as a possible motion. (See Figure 8 and associated text in ref 11.)

$T_{1\rho}$(C) and n_2/n_1. The ratio of intensities of the second to first dipolar sidebands for the protonated aromatic carbon of atactic polystyrene is 1.20 (Table IX). After

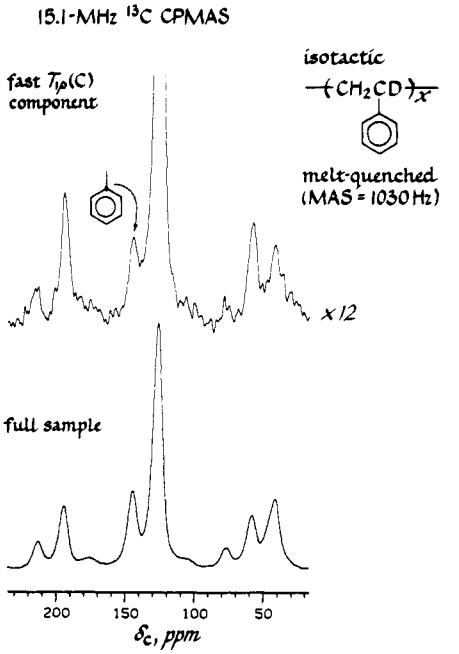

Figure 12. Magic-angle cross-polarization 15.1-MHz ^{13}C NMR spectra of isotactic poly(styrene-α-*d*) under slow-speed conditions (bottom). The spectrum of the short-T_1(C) component is shown at the top of the figure.

a 30-ms 60-kHz spin-lock delay during the carbon preparation step of the rotational dipolar echo experiment (Figure 2, t_3 = 30 ms), the observed n_2/n_1 ratio increases to 1.31. This quantity is identified as $[n_2/n_1]_d$ in Table IX. Similar changes in the dipolar sideband pattern following carbon spin-lock delays have been observed before for some modified polycarbonates.[10,11] These changes are associated with dynamic heterogeneity. That is, rings with little motion survive the spin lock and make a proportionately greater contribution to the sideband pattern after the delay than before it. The same sort of heterogeneity is also shown by the polystyrene aliphatic methine carbon CH dipolar n_2/n_1, which increases some 5% after a 30-ms 60-kHz spin lock (from 1.24 to 1.31), even though the methine carbon $\langle T_{1\rho}(C)\rangle$ at this H_1(C) is sufficiently long that only about 10% of the total polarization decays.[1]

As shown in Figure 8, about half the rings in poly(*p*-methylstyrene) with short T_1(C)'s, which we have established to be undergoing megahertz-rate flips, also survive the carbon spin-lock delay. Megahertz-rate ring flips reduce the observed n_2/n_1 dipolar sideband ratio. The contribution of these rings to $[n_2/n_1]_d$ can be estimated by using the value of $f(c)$ from T_1(C) experiments (Table VI) and the calculated n_2/n_1 for ring flips (0.48). Removing

Table X
Protonated Aromatic $\langle T_{1\rho}(C)\rangle$'s of Some Polystyrenes Scaled by the Amplitude of Root-Mean-Square Angular Fluctuations Deduced from Experimental Dipolar Rotational Sideband Intensities

system	37-kHz $\langle T_{1\rho}(C)\rangle$,[a] ms	n_2/n_1 [b]	$[n_2/n_1]_0$* [c]	θ	$\langle T_{1\rho}(C)\rangle \sin^2\theta$
poly(*p*-*tert*-butylstyrene)	6.2	1.04	1.11	23	0.89
poly(*p*-isopropylstyrene)	8.8	1.08	1.15	21	1.06
polystyrene[d]	11.2	1.20	1.25	18	1.00
poly(*p*-methylstyrene)	11.7	1.20	1.25	18	1.04
poly(α-methylstyrene)	19.0	1.30	1.30	16	1.35
poly(styrene-*co*-sulfone)	22.0	1.32[e]	1.32	15	1.38
poly(*o*-chlorostyrene)	37.0	1.34	1.34	14	2.02

[a] Straight-line fit to observed decay between 0.05 and 1.00 ms after the turn off of H_1(H). [b] Ratio of intensities of second to first dipolar rotational sidebands. [c] Ratio of intensities of second to first dipolar rotational sidebands with contributions from rings undergoing megahertz-rate flips removed. [d] Atactic, quenched, high-molecular-weight material. [e] Contributions to n_1 from the nonprotonated aromatic carbon removed, assuming $n_1/n_0 = 0.13$ for that carbon, the same ratio as is observed for polystyrene.

this contribution for atactic polystyrene results in a n_2/n_1 dipolar sideband ratio of 1.37. Similarly corrected values ($[n_2/n_1]_d$*'s in Table IX) are observed for isotactic polystyrenes that have some crystallinity, as well as for a completely crystalline model compound, *para*-isopropoxybenzoic acid. The latter compound has no ring motion as indicated by an extremely long $\langle T_{1\rho}(C)\rangle$.

Values of n_2/n_1 (after zero spin-lock delay) with contributions from ring flips removed are presented in Table X for seven polystyrenes. These values are identified as $[n_2/n_1]_0$*. For all seven polymers, short $\langle T_{1\rho}(C)\rangle$'s go with small values of $[n_2/n_1]_0$*, and long $\langle T_{1\rho}(C)\rangle$'s go with values of $[n_2/n_1]_0$* close to 1.4.

Discussion

Large-Amplitude High-Frequency Ring Motion. About 7% of the rings of atactic polystyrene are engaged in 180°-flip megahertz-rate motion. We know the motion of this 7% fraction is large amplitude because of the extent of collapse of the dipolar tensor for the protonated aromatic carbons. We know the motion is in the 10-MHz regime because the observed T_1(C) of this fraction is close to the T_1 minimum of about 25 ms at 15 MHz for a CH carbon.[24] And, finally, we know the motion is actually 180° flips of the rings (perhaps superimposed on some smaller amplitude wiggling) because the chemical shift tensor of the on-axis nonprotonated aromatic carbon of this fraction is unchanged by the motion.

The fraction of rings doing the flipping in polystyrene is unaffected by either configurational or conformational defects in the chain. Thus, atactic and isotactic amorphous polystyrenes have about the same concentration of flippers. Atactic polystyrenes, either melt quenched or precipitated from a solvent at 35 °C, also have the same concentration of flippers. In the latter comparison, both polymers have had their unperturbed equilibrium concentration of conformational states locked into the glass, but at temperatures 70 °C apart. The higher temperature distribution has the greater concentration of conformational defects, but this has no influence on flippers. The only effect on the concentration of flippers of thermal conditioning of polystyrenes occurs when isotactic material is made partially crystalline. Even in that situation it appears that flipping rings remain active in the amorphous regions of the polymer.

The ring flips appear to be part of a cooperative motion that includes the polymer main chain. About 5% of the methine CH sites in atactic polystyrene are involved in a reasonably large-amplitude megahertz-rate rotational reorientation (Figure 7), with about a third of those methine carbons having a particularly short T_1(C). Naturally, it is impossible to prove that the same sites in the glass having ring flippers also have main chains with short T_1(C)'s, but such a speculation is at least plausible and leads us to a suggestion for the origin of the ring flippers.

We assign the ring flippers to those sites in the glass where, by chance, packing of chains has resulted in main-chain flexibility. High-frequency main-chain wiggling then leads to a relatively low barrier to phenyl-ring rotation. Single-chain calculations[21,23] confirm that when steric parameters are used that confer flexibility on the main chain, phenyl-group rotational barriers are on the order of 10 kcal/mol and consistent with megahertz-rate jumps. If rigid-chain parameters are used, the calculated barrier to phenyl rotation increases to 100 kcal/mol.[21] Main-chain flexibility also explains the increased kilohertz-rate wiggling, which produces effective ring $\langle T_{1\rho}(C)\rangle$ relaxation at the ring-flip sites (Table V).

Local free volume in the glass that allows rings some lattitude in rotational motion may be part of what makes the main chains flexible. This microscopic free volume is not lost by low-temperature annealing of polystyrene since no conformational redistribution of the main chain occurs. Thus, neither $f(c)$, T_1(C), nor $T_{1\rho}$(C) of atactic polystyrene is sensitive to annealing. The free volume that is lost by low-temperature annealing of polystyrene must involve reorganization of larger domains.

The assignment of ring flippers to sites selected on an entropic chain-packing basis makes understandable the insensitivity of $f(c)$ to annealing of atactic polystyrene. The selection of sites for flips is not critically linked to defects of any sort, so programs designed to eliminate or reduce conformational or configurational defects naturally have little or no effect. Bulky substituents in the ring para position can have a sizable effect, however. In this situation, para substituents make room for their attached main chains in the melt, and this freedom translates into sufficient main-chain flexibility in the glass to produce a low-energy barrier to ring flipping. These packing barriers, however, are still not sufficiently low in energy to permit freely rotating rings. That is, on say a 90° excursion from its equilibrium position, a ring at a flip-permissible site encounters a significant repulsive interchain steric interation so that the residence time at this orientation is nil. In short, ring flipping is a highly restricted form of rotation.

While bulky para substituents can aid main-chain flexibility and promote ring flippers, main-chain substitution can have the opposite effect. Thus, poly(α-methylstyrene) with its altered interchain packing parameters has no sites where ring flips are allowed, even though free volume and single-chain flexibility considerations all seem similar to those of polystyrene.[21] Poly(styrene-*co*-

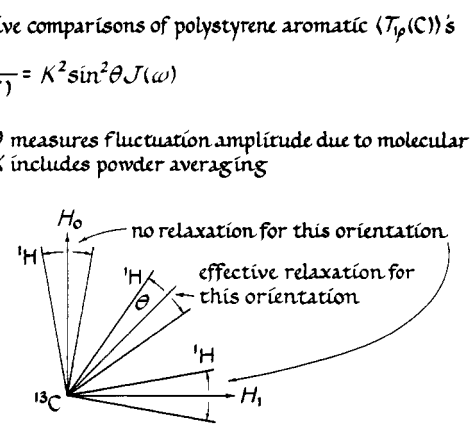

Figure 13. Geometrical considerations for a CH vector giving rise to $T_{1\rho}$(C) relaxation in a solid by restricted rotational reorientation.

sulfone) may also suffer from a stiffened main chain (resulting in no flippers), although the absence of flippers here may be due to intrachain steric hindrance of ring rotation, just as is almost surely the case for poly(*o*-chlorostyrene).

Small-Amplitude Low-Frequency Ring Motion. Even ignoring those sites engaged in ring flipping, measurable ring motion exists in polystyrenes. This can be seen both in the short aromatic $T_{1\rho}$(C)'s after T_1(C) delays to remove the effects of ring flips (Table V) and in ratios of dipolar sideband intensities $[n_2/n_1]_0$* which are less than the ratio observed for crystalline materials such as *p*-isopropoxybenzoic acid (Tables IX and X). The weak but still measurable H_1(C) dependence of the ring $\langle T_{1\rho}(C)\rangle$'s (Table III) establishes the presence of a distribution of frequencies with an average value, perhaps, of the order of 100 kHz. For a 100-kHz free rotor in the solid, we expect[25] a 40-kHz $\langle T_{1\rho}(C)\rangle$ of 1 ms. The observed value is about 10 ms, suggesting that the ring motion in question is restricted to an average angular displacement of 30–40°. The fact that both $T_{1\rho}$(C) and $[n_2/n_1]_0$* show the influence of this small-amplitude low-frequency motion suggests a simple connection between them. That is, the same cooperative kilohertz-regime motions responsible for $T_{1\rho}$(C) must also be responsible for the partial averaging of the aromatic CH dipolar tensor.

For the protonated aromatic carbons of polystyrenes under rotational reorientation, we propose $T_{1\rho}^{-1}(C) = K^2(\sin^2\theta)J(\omega)$, where K^2 is a constant (which includes powder averaging in the solid), $\sin^2\theta$ is the average dipolar fluctuation orthogonal to the applied radio-frequency field (Figure 13), and $J(\omega)$ describes the spectral density associated with the ring motion at the carbon rotating-frame Larmor frequency,[26] in this instance, 37 kHz. The $J(\omega)$'s for all ring-substituted polystyrenes appear to be about the same (Table III). If we assume ring rotation only occurs about the ring C_2 axis, then the relative $T_{1\rho}$(C)'s should be a simple function of the amplitude of the ring motion as measured by θ. These amplitudes can be estimated from the reduction in the dipolar CH patterns as characterized by the n_2/n_1 ratios (or $[n_2/n_1]_0$* ratios, where appropriate), if we assume that the motion which reduces n_2/n_1 (Table VIII) is also responsible for the $T_{1\rho}$ relaxation. The results of such a comparison for seven substituted polystyrenes are shown in Table X. The product of $\sin^2\theta$ and $\langle T_{1\rho}(C)\rangle$ is indeed roughly constant for all seven polymers. The product for the first six polymers in Table X is constant to within about 50% even though the $\langle T_{1\rho}(C)\rangle$'s themselves vary by a factor of 4. Based on rms[27] values of θ, the ring rotations generate total angular displacements of about 40° (for substituents in the ortho position) to 70° (for bulky nonpolar substituents in the para position.

We have chosen motion about the C_2 axis to model ring motion and achieve the correlation between $\sin^2\theta$ and $\langle T_{1\rho}(C)\rangle$ shown in Table X. Small-amplitude wiggling can equally well be modeled by aromatic CH motion on a circle or sphere. The latter models could be thought of as representing, in an approximate way, rotational excursions by a ring as it tracks its attached main chain through complicated motions.

We recognize that polystyrenes are dynamically heterogeneous (even ignoring ring flippers). Thus, both $T_{1\rho}$(C)'s and angular displacement fluctuation parameters must reflect averages over the entire sample. Of course, the observed $\langle T_{1\rho}(C)\rangle$ is the weighted average of all the $T_{1\rho}$(C)'s present.[2] Since the n_2/n_1 ratio has an approximately linear dependence on total angular displacement (and is not critically model dependent), the observed root-mean-square fluctuation parameter, θ, is also a simple weighted average. In part, the correlation of Table X (between $\langle T_{1\rho}(C)\rangle$ and $\sin^2\theta$) succeeds because we ignore details of the distributions of motions. Thus, whether polystyrene has a fraction of highly mobile rings with the remainder less mobile, or whether all rings have an intermediate mobility, becomes immaterial. Both situations result in comparable average values for $\langle T_{1\rho}(C)\rangle$ and θ. The correlation of Table X fails to the extent there remain large-amplitude high-frequency motions (after removal of ring flips) which reduce n_2/n_1 but do not contribute to $T_{1\rho}$(C), or 5–10° small-amplitude low-frequency motions which can make significant contributions to $\langle T_{1\rho}(C)\rangle$ but have only a minor effect on n_2/n_1. The correlation also suffers from the presence of large-amplitude motions near 10 kHz which have effects on n_2/n_1 not well represented by our calculations, which assume all motion is faster than dipolar coupling. (We suspect this limitation is not severe since large-amplitude motions tend to be high rather than low frequency.)

Two technical details remain that can also affect the quality of the correlation between $\langle T_{1\rho}(C)\rangle$ and $\sin^2\theta$. First, the longer $\langle T_{1\rho}(C)\rangle$'s undoubtedly have some spin–spin contribution. We can estimate[1] a 37-kHz $\langle T_{IS}$(ADRF)$\rangle$ of 100 ms for a static ring with adjacent protons only three bonds apart and have measured a value of 83 ms for *p*-isopropoxybenzoic acid. All the rings of the polystyrenes examined have proton local fields partially averaged by molecular motion so a $\langle T_{IS}$(ADRF)$\rangle$ of 100 ms at 37 kHz is probably a lower limit. Nevertheless, this means the $\langle T_{1\rho}(C)\rangle$'s of poly($\alpha$-methylstyrene) and poly(*o*-chlorostyrene) have 20–30% spin–spin character, and the correlation of Table X is not as good as first appears.

The other technical detail is our choice of WAHUHA scaling factor. The width of the observed aromatic CH dipolar pattern for crystalline materials like dimethoxybenzene[10] is less than expected for a rigid CH pair but agrees with what is calculated with an apparent WAHUHA scaling factor of 0.44. (The theoretical scaling factor[15] is 0.58, which is close to what we have measured for the scaling of proton chemical shifts in liquids.) The reduced scaling factor is not the result of an NMR instrumental effect but rather is due to a genuine reduction in dipolar coupling. This reduction in effective dipolar coupling for solids occurs because the NMR experiment depends on $\langle r^{-3}\rangle^2$, where r is the CH internuclear separation and the bracket indicates a time average. Ultrahigh-frequency motions in crystals[28] can have a significant effect on av-

eraging the dipolar coupling[29] between CH and NH, with a lesser effect on the coupling between CC and CN. A 20% reduction in dipolar coupling (corresponding to a 6% apparent increase of CH and NH bond lengths) has been observed in a variety of solids NMR experiments, some of which do not involve WAHUHA decoupling.[30,31] These reductions in dipolar coupling occur for systems normally considered rigid. The presence of ultrahigh-frequency lattice motions means that in solids experiments using WAHUHA decoupling, the theoretical scaling factor cannot be used. However, because the ultrahigh-frequency elastic properties of most organic solids are about the same,[28] we can assign the same apparent (or effective) WAHUHA scaling factor to characterize organic solids of the same general type. Then, differences in glassy polymer CH and CH_3 dipolar patterns from those observed for the appropriate nominally rigid model systems must be due to kilohertz- and megahertz-regime motions.

We have no way to *predict* the apparent WAHUHA scaling factor for any particular system. A scaling factor of 0.42 gives rise to a rigid CH n_2/n_1 of 1.50, a value that has been observed for several crystalline small molecules,[10] as well as for aromatic polymers with little motion, and for poly(styrene-*co*-sulfone) (Table VII, row 5).[11] This is the scaling factor we have used in Tables VII–X. However, the limiting n_2/n_1 for many polystyrenes appears to be about 1.40 (Table IX, last column). If we were to use the latter value (and so a smaller scaling factor), the estimate for θ for poly(*o*-chlorostyrene), for example, would be about half of that of Table X and the correlation between $\langle T_{1\rho}(C)\rangle$ and $\sin^2\theta$ substantially improved. At this point, we choose not to draw such fine distinctions. We anticipate improvements in the dipolar rotational echo experiment (particularly with respect to percentage of refocused echo) and a greater catalog of model systems and so expect future minor adjustments in apparent scaling factors for specific systems.

Mechanism of Low-Frequency Ring Motion. Although we have specified the amplitude of ring oscillation in polystyrene, we have said nothing about the *mechanism* of the motion. In particular, we have not established whether ring oscillation occurs by diffusive small incremental steps or by jumps that cover the same total angular amplitude in one or two big steps. For the ring-substituted polystyrenes of Tables III and X, we have established that the average correlation time for cooperative ring oscillation about the C_2 axis does not vary, even though the amplitude of the oscillation changes by about a factor of 2. One way of thinking of the correlation time for motion is as a coherence or memory time. This parameter measures the time required for the loss of memory of a particular spatial location as a result of motion.

Normally, for small-step diffusive motion, the more restricted in space the motion is, the shorter the coherence time. This effect can be visualized by a simple analogy. Imagine that you are standing in the corner of a checkerboard and permitted to make random jumps only between the red squares near one corner. The probability of finding yourself on any one of those red corner squares is soon the same as for any other, regardless of which one you started from. But the time to reach this same state of equal probabilities is considerably longer if you can move over the entire checkerboard, assuming your jump time and length are the same. To explain the observed equality of correlation times for the ring oscillations of the ring-substituted polystyrenes by a small-step diffusive motion, one must assume that as the motion becomes restricted (by the effects of ring substitution on glassy packing), it also slows down. The small-step jump time does not remain the same.

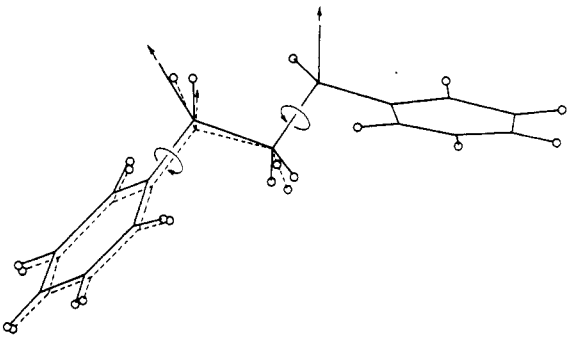

Figure 14. Schematic representation of a polystyrene main-chain rotational reorientation in which the rings do not rotate, for the special situation when two bond directions are collinear.

While this assumption is not totally implausible, it does force a physical picture of cooperative molecular motion in which each small step of the main chain (a step which could be as small as, say, 0.1 angular degree with a jump time of a fraction of a nanosecond) is exactly geared to the corresponding small step of the ring. The two motions cannot be independent because there would then be no way to explain the "slowing down" phenomenon required by equal correlation times for low-frequency cooperative motions. We see no physical interaction in the glass to ensure such a fine-scale ratcheting. Rather, we feel the evidence points to ring motion in polystyrenes by big jumps. The ring jumps are connected to main-chain motions and occur when the latter relieve local steric constraints in the glass. The time required to complete a jump once started is very short and does not influence our NMR measurements. The time between jumps is determined by the main-chain motion and is about 10 μs for the whole series of ring-substituted polystyrenes. Since the jumps are large, the time between them is the coherence time.

Main-Chain Motion. Both the $\langle T_{1\rho}(C)\rangle$ and the dipolar sideband patterns of main-chain aliphatic CH's show the effect of molecular motion. However, interpreting changes in $\langle T_{1\rho}(C)\rangle$ from one polystyrene to another in terms of motion, as was done for the rings, is difficult because of a greater spin–spin contribution to the main-chain carbon relaxation than to the ring-carbon relaxation. Nevertheless, some careful comparisons have been made. For example, the spin–lattice or motional contribution to the main-chain $\langle T_{1\rho}(C)\rangle$ for both polystyrene and poly(*o*-bromostyrene) are comparable (Table IV, ref 1), as are the aliphatic CH dipolar patterns (not shown). This is true even though the ring motions evaluated by the same parameters are clearly different.

We interpret such results in terms of the presence of at least two classes of motions in polystyrenes. The first involves rotations about the ring C_2 axes (in cooperation with main-chain reorientation) and has been described in the previous two sections. This class of motions includes both flips and wiggles. The second class we propose is a cooperative main-chain motion in which the rings undergo limited translations but no rotations. This motion is insensitive to ring substitution and is responsible in part for the aliphatic-carbon motional contribution to $\langle T_{1\rho}(C)\rangle$. Such a motion in the kilohertz frequency range can become important for main-chain $T_{1\rho}(C)$ relaxation when the phenyl rings are rotationally constrained. This motion is illustrated in Figure 14 for a special orientation of a $-CHPhCH_2CHPh-$ segment of a polystyrene chain. The general motion involves cooperative (but, on a microsecond

time scale, not necessarily simultaneous[32]) rotation about all four bonds separating two phenyl groups, resulting in no significant net rotation of either ring. Translation of segment ends is necessary, however, as in motions proposed by Helfand for long-chain alkanes.[33]

In addition to a dependence on ring constraints in the glass implicit in this ring-translation motion, polystyrene main-chain motions are also dependent on *intra*chain interactions. For example, insertion of a sulfone unit into the main chain causes a considerable stiffening in the low-frequency regime as measured by an increase relative to polystyrene of more than a factor of 2 in the H_1(C)-dependent[1,3] main-chain $\langle T_{1\rho}(C)\rangle$'s (Table II). This behavior is consistent with that in solution as measured[19] by ^{13}C T_1's. Such parallels are not the rule, however. By contrast with the observation of a significant increase in flexibility relative to polystyrene for poly(phenylthiirane) in solution,[20] we observe no change in main-chain $\langle T_{1\rho}(C)\rangle$'s. While the presence of a sulfur link in the polystyrene main-chain may tend to localize the cooperativity implicit in motion such as that illustrated in Figure 14, we have not been able to detect this effect in diminished $T_{1\rho}$(C) dispersions.

Finally, we note that the 2.5-ms $\langle T_{1\rho}(C)\rangle$ for the methylene carbons of poly(α-methylstyrene) indicates only a modestly increased low-frequency motion (compared to the 5-ms value for polystyrene) since the former $\langle T_{1\rho}(C)\rangle$ has an increased spin–spin component.[1]

Comparison of Results of ^{13}C and ^{2}H NMR of Polystyrene. Spiess[34] has examined ring- and main-chain specifically deuterated atactic polystyrenes using ^{2}H NMR.[35] His line shapes are in reasonable agreement with our rotational dipolar spin-echo ^{13}C NMR line shapes. In particular, Spiess observes a minor short-$T_1(^2H)$ component with a collapsed aromatic quadrupolar tensor, consistent with the presence of 180° flips. The observed line shape for this component appears to be missing some of the well-defined shoulders that would be present if 180° flips were the only motion. That is, the deuterium line shape for the short-T_1 component is consistent with the presence of additional wiggles superimposed on the C_2-axis flips, just as required by the ^{13}C results (Figure 11).

The line shape of the long-$T_1(^2H)$ component also has deviations from the calculated aromatic quadrupolar static pattern, consistent with the presence of small-amplitude motions, although Spiess has chosen not to interpret these effects. He has, however, reported the presence of low-kilohertz regime motions for polystyrene from deuterium spin-alignment experiments for both ring and main chain.[36]

Connection between Molecular Motion in Polystyrenes and Mechanical Properties. A small fraction of rings in many of the polystyrenes examined engage in 10-MHz 180° flips. Ring flips apparently require main-chain flexibility, which, in turn, is consistent with the observation that a few main-chain sites are also undergoing megahertz-rate rotational reorientation. Ring flipping is a restricted rotation. We have presented arguments above supporting the notion that the origin of the restrictions ultimately is interchain packing in the glass. Flipping of a ring therefore demands some distortion of the lattice as a polystyrene ring pushes chains or other rings out of the way during the flip. The motion is therefore mechanically active. We assign the weak tan-δ γ transition (1 Hz at −120 °C) of mechanical loss spectra of polystyrene[37] to cooperative ring flips (10 MHz at 25 °C). This assignment makes a plausible connection between the observed mechanical and NMR frequencies. Experimental[38,39] and calculated[21] activation energies for the γ transition of atactic polystyrene are of the order of 10 kcal/mol. Thus, for a motion with a frequency of 1 Hz at −120 °C, we can expect at 25 °C a frequency of about (1 Hz) × exp(−5000(1/298 − 1/153)) = 8 MHz, if indeed the character of the motion is unchanged between −120 and +25 °C.

Table XI
Comparison of Ring-Motion NMR Parameters and Gas Diffusivity for Some Polystyrene Films

system	37-kHz $\langle T_{1\rho}(C)\rangle$,[a] ms	$f(c)$[b]	diffusivity[c] ($\times 10^6$), cm^2 s^{-1} H_2	CO
poly(*p*-*tert*-butylstyrene)	6.2	0.11	4.4	0.39
polystyrene[d]	11.2	0.07	1.8	0.023
poly(*o*-chlorostyrene)	37.0	0.06	0.60	0.01

[a] Straight-line fit to observed decay between 0.05 and 1.00 ms after the turn off of H_1(H). [b] Mole fraction of rings undergoing megahertz-rate 180° flips (see Table VI). [c] From thin-film time-lag measurements (ref 41). [d] Atactic, melt-quenched, high-molecular-weight material.

From both $T_{1\rho}$(C) measurements and dipolar sideband patterns the rings and main chains of polystyrenes are also engaged in a variety of small-amplitude rotational reorientations between 10 kHz and several hundred kilohertz. (There may well be motions at lower frequencies than 10 kHz but our measurements are insensitive to them.) The lowest frequency of these motions is necessarily cooperative, since small-amplitude local motion cannot also be low frequency. We assign the broad, intense tan-δ β transition[37] (1 Hz at −60 to +20 °C) to cooperative ring- and main-chain restricted oscillations.

These assignments make a molecular identification of the only two major sub-T_g transitions in the anelastic mechanical loss response of polystyrenes.

Molecular Motion in Polystyrenes and Gas Diffusivity. Recently, Pace and Datyner[40] advanced a molecular theory of diffusion that correlates the diffusivity of simple gases in a polymeric matrix with cooperative motions of the chains. This theory explains how macroscopic transport described by the diffusivity can be as much as 6 orders of magnitude less than anticipated from predictions based on the time scale of the microscopic motion of the gas molecule in the polymer. It appears that the limiting process for diffusion in polymers involves the relatively slow cooperative motion of chains, allowing gas molecules to progress from one region of local mobility to another. Pace and Daytner estimated the time scale for this process based on the size of the penetrant gas molecule and an assumed interchain interaction potential. For molecules like CO and H_2, the frequencies of polymer motions important to diffusion are predicted[40] to be in the range 10^5–10^8 Hz.

We have observed[41] H_1(C)-dependent $\langle T_{1\rho}(C)\rangle$'s for a variety of poly(vinyl chloride) diffusion systems and made a connection between microscopic molecular chain motion and macroscopic CO/H_2 gas diffusivities. A similar connection has been established between sub-T_g mechanical loss behavior (characterizing microscopic molecular motion) and CO_2 and O_2 gas transport properties in polyester films.[42] In this paper, we have established that microscopic motions in polystyrenes (wiggles and flips) range in frequency from 10^4 to 10^7 Hz. We should therefore expect a simple correlation between polystyrene motional parameters determined by ^{13}C NMR and diffusivities for CO and H_2 in polystyrene films and membranes. A direct correlation is, in fact, observed (Table XI).

Acknowledgment. We thank L. Monnerie for several helpful comments concerning main-chain motions in polystyrenes. Conclusions about the origins of ring flips in polystyrenes benefited from extended discussions with R. Yaris, J. Skolnick, D. Perchak, and A. Tonelli. This work was supported in part by Grant DMR-8007025 from the Polymer Division of the National Science Foundation.

Registry No. Atactic polystyrene, 9003-53-6; isotactic polystyrene, 25086-18-4; poly(*p*-bromostyrene), 24936-50-3; poly(*p*-chlorostyrene), 24991-47-7; poly(*p*-nitrostyrene), 24936-54-7; poly(*p*-isopropylstyrene, 30872-09-4; poly(α-methylstyrene), 25014-31-7; poly(*o*-bromostyrene), 27290-16-0; poly(*m*-bromostyrene), 25584-47-8; poly(*p*-*tert*-butylstyrene), 26009-55-2.

References and Notes

(1) Schaefer, J.; Sefcik, M. D.; Stejskal, E. O.; McKay, R. A. *Macromolecules*, following paper in this issue.
(2) Stejskal, E. O.; Schaefer, J.; Steger, T. R. *Faraday Soc., Symp.* **1979**, *13*, 56.
(3) Schaefer, J.; Stejskal, E. O.; Steger, T. R.; Sefcik, M. D.; McKay, R. A. *Macromolecules* **1980**, *13*, 1121.
(4) Maricq, M.; Waugh, J. S. *J. Chem. Phys.* **1979**, *70*, 3300.
(5) Hester, R. K.; Ackerman, J. L.; Neff, B. L.; Waugh, J. S. *Phys. Rev. Lett.* **1976**, *36*, 1981.
(6) Stoll, M. E.; Vega, A. J.; Vaughan, R. W. *J. Chem. Phys.* **1976**, *65*, 4093.
(7) Dixon, W. T. *J. Chem. Phys.* **1982**, *77*, 1800.
(8) Munowitz, M. G.; Griffin, R. G.; Bodenhausen, G.; Huang, T. H. *J. Am. Chem. Soc.* **1981**, *103*, 2529.
(9) Munowitz, M. G.; Griffin, R. G. *J. Chem. Phys.* **1982**, *76*, 2848.
(10) Schaefer, J.; McKay, R. A.; Stejskal, E. O.; Dixon, W. T. *J. Magn. Reson.* **1983**, *52*, 123.
(11) Schaefer, J.; Stejskal, E. O.; McKay, R. A.; Dixon, W. T. *Macromolecules*, in press.
(12) Opella, S. J.; Frey, M. H.; DiVerdi, J. A. *J. Magn. Reson.* **1980**, *37*, 165.
(13) Torchia, D. A. *J. Magn. Reson.* **1978**, *30*, 613.
(14) Waugh, J. S.; Huber, L. M.; Haeberlen, U. *Phys. Rev. Lett.* **1968**, *20*, 180.
(15) Haeberlen, U. *Adv. Magn. Reson., Suppl. 1* **1976**, 1.
(16) Herzfeld, J.; Berger, A. E. *J. Chem. Phys.* **1980**, *73*, 6021.
(17) Moore, J. A., Ed. "Macromolecular Syntheses"; Wiley: New York, 1977; Collect. Vol. 1, pp 1-3.
(18) Van, N. B.; Noel, C. *J. Polym. Sci., Polym. Chem. Ed.* **1976**, *14*, 1627.
(19) Cais, R. E.; O'Donnell, J. H.; Bovey, F. A. *Macromolecules* **1977**, *10*, 254.
(20) Cais, R. E.; Bovey, F. A. *Macromolecules* **1977**, *10*, 752.
(21) Tonelli, A. E. *Macromolecules* **1973**, *6*, 682.
(22) See Figure 8 of ref 11.
(23) Hägele, P. C.; Beck, L. *Macromolecules* **1977**, *10*, 213.
(24) Doddrell, D.; Glushko, V.; Allerhand, A. *J. Chem. Phys.* **1972**, *56*, 3683.
(25) McCall, D. W. *Acc. Chem. Res.* **1971**, *4*, 223.
(26) Abragam, A. "The Principles of Nuclear Magnetism"; Oxford University Press: London, 1961; p 565.
(27) In this paper the mean is taken of the square of the sines of the angles rather than the squares of the angles themselves to obtain a root mean square. Arcsin root mean sine square is a more accurate term. For small angles where $\sin\theta \sim \theta$, the two means are the same.
(28) Van Krevalen, D. W. "Properties of Polymers"; Elsevier: New York, 1976; p 267.
(29) Szeverenyi, N. M.; Vold, R. R.; Vold, R. L. *Chem. Phys.* **1976**, *18*, 23.
(30) Stoll, M. E.; Vega, A.; Vaughan, R. W. *J. Chem. Phys.* **1978**, *69*, 5458.
(31) Stark, R. E.; Haberkorn, R. A.; Griffin, R. G. *J. Chem. Phys.* **1978**, *68*, 1996.
(32) Skolnick, J.; Helfand, E. *J. Chem. Phys.* **1980**, *72*, 5489.
(33) Helfand, E. *J. Chem. Phys.* **1971**, *54*, 4651.
(34) Spiess, H. W. *Colloid Polym. Sci.* **1983**, *261*, 193.
(35) Spiess, H. W. *J. Chem. Phys.* **1980**, *15*, 6755.
(36) Spiess, H. W., private communication.
(37) See, for example: McCrum, N. G.; Read, B. E.; Williams, G. "Anelastic and Dielectric Effects in Polymeric Solids"; Wiley: New York, 1967; p 410.
(38) Yano, O.; Wada, Y. *J. Polym. Sci., Part A-2* **1971**, *9*, 669.
(39) Hedvig, P., "Dielectric Spectroscopy of Polymers"; Adam Hilyer, Ltd.: Bristol, 1977; p 114.
(40) Pace, R. J.; Datyner, A. *J. Polym. Sci., Polym. Phys. Ed.* **1979**, *17*, 437.
(41) Sefcik, M. D.; Schaefer, J.; May, F. L.; Raucher, D.; Dub, S. M. *J. Polym. Sci., Polym. Phys. Ed.* **1983**, *21*, 1055.
(42) Light, R. R.; Seymour, R. W. *Polym. Eng. Sci.* **1982**, *22*, 857.
(43) Poly(styrene-*co*-sulfone) is not a systematic name, but rather a convenient representation for the constitution of the polymer whose structural formula is shown in Figure 9.

Carbon-13 $T_{1\rho}$ Experiments on Solid Polymers Having Tightly Spin-Coupled Protons

Jacob Schaefer,* M. D. Sefcik, E. O. Stejskal, and R. A. McKay

Monsanto Company, Physical Sciences Center, St. Louis, Missouri 63167.
Received July 25, 1983

ABSTRACT: A nine-step procedure is established for measuring the cross-polarization transfer rate from protons in local dipolar fields to carbons in an applied radio-frequency field. This measurement permits a determination of the relative contributions of spin and motional dynamics to average carbon rotating-frame relaxation times ($\langle T_{1\rho}(C)\rangle$'s) even in situations when both mechanisms are important. The $\langle T_{1\rho}(C)\rangle$'s at 37 kHz for the methylene carbons of polycrystalline glycine, high-density polyethylene, poly(oxymethylene), and hexadecane contained in a urea clathrate are all dominated by spin dynamics, while those of dipalmitoylphosphatidylcholine, poly(α-methylstyrene), and an atactic melt-quenched polystyrene reflect substantial motional contributions. A phenomenological expression for calculating the cross-polarization transfer rate for methylene carbons in amorphous or polycrystalline materials is also proposed. Calculated values are in reasonable agreement with experiment for nine different solid systems, all of which have tightly spin-coupled protons. In many situations, this simple calculation will permit an estimate of spin–spin contributions to observed carbon rotating-frame relaxation times without elaborate experiments.

Introduction

In a recent discussion of the molecular dynamics of chemically modified polycarbonates, Yee and Smith[1] noted the absence of any clear correlation between the results of dynamic mechanical spectroscopy of these polycarbonates and broad-line proton NMR of the same materials. The source of this difficulty is not hard to find. Molecular motions of the polymer modulate the dipolar interactions on which all NMR relaxation parameters depend. These parameters therefore reflect the inherent

0024-9297/84/2217-1118$01.50/0